◆ Human Brain Mapping 35:1179–1189 (2014) ◆

Template-Based Approach for Detecting Motor Task Activation-Related Hyperperfusion in Pulsed ASL Data

Jan Petr,[1,2,3,4]* Jean-Christophe Ferré,[1,2,3,5] Hélène Raoult,[1,2,3,5] Elise Bannier,[1,2,3] Jean-Yves Gauvrit,[1,2,3,5] and Christian Barillot[1,2,3]

[1]*INRIA, Team VisAGeS, Campus Universitaire de Beaulieu, Rennes, France*
[2]*INSERM, Unit VisAGeS U746, Campus Universitaire de Beaulieu, Rennes, France*
[3]*University of Rennes I, CNRS, Unit VisAGeS U746, IRISA, Campus Universitaire de Beaulieu, Rennes, France*
[4]*Helmholtz-Zentrum Dresden-Rossendorf, Dep. of Positron Emission Tomography, Institute of Radiopharmaceutical Cancer Research, Dresden, Germany*
[5]*CHU Rennes, Department of Neuroradiology, University Hospital of Rennes, Rennes, France*

Abstract: Arterial spin labeling (ASL) permits the noninvasive measurement of quantitative values of cerebral blood flow (CBF) and is thus well adapted to study inter- and intrasubject perfusion variations whether at rest or during an fMRI task. In this study, a template approach to detect brain activation as a CBF difference between resting and activated groups was compared with a standard generalized linear model (GLM) analysis. A basal perfusion template of PICORE-Q2TIPS ASL images acquired at 3T from a group of 25 healthy subjects (mean age 31.6 ± 8.3 years) was created. The second group of 12 healthy subjects (mean age 28.6 ± 2.7 years) performed a block-design motor task. The template was compared with the mean activated image of the second group both at the individual and at the group level to extract activation maps. The results obtained using a GLM analysis of the whole sequence was used as ground truth for comparison. The influences of spatial normalization using DARTEL registration and of correction of partial volume effects (PVE) in the construction of the template were assessed. Results showed that a basal perfusion template can detect activation-related hyperperfusion in motor areas. The true positive ratio was increased by 2.5% using PVE-correction and by 3.2% using PVE-correction with DARTEL registration. On average, the group comparison presented a 2.2% higher true positive ratio than the one-to-many comparison. *Hum Brain Mapp 35:1179–1189, 2014.*

Key words: arterial spin labeling; motor activation; template; perfusion; functional MRI; ASL

INTRODUCTION

Arterial spin labeling (ASL) is a completely noninvasive MRI method that measures brain perfusion by magnetically labeling blood in brain-feeding arteries [Detre et al., 1992; Parkes and Detre, 2004]. The main advantage of ASL is its ability to obtain quantitative values of cerebral blood flow (CBF) without using contrast agent or ionizing radiation. The reproducibility of CBF quantification makes ASL

*Correspondence to: Jan Petr, HZDR, PET Center, Institute of Radiopharmaceutical Cancer Research, POB 51 01 19, 01314 Dresden, Germany. E-mail: j.petr@hzdr.de

Received for publication 2 April 2012; Revised 31 October 2012; Accepted 24 November 2012

DOI: 10.1002/hbm.22243

Published online 13 February 2013 in Wiley Online Library (wileyonlinelibrary.com).

a promising method for diagnosis based on inter- and intra-subject perfusion comparison [Chen et al., 2011; Petersen et al., 2010; Wang et al., 2011]. The main drawback of ASL is its low signal-to-noise ratio (SNR) and poor spatial resolution, ranging between 3×3 mm^2 and 4×4 mm^2 per pixel in-plane and 5 and 8 mm slice thickness. A useful way of overcoming the SNR limitation is to implement ASL at high-field strength, and to use multi-channel coils, parallel acquisition techniques and dedicated software processing [Ferré et al., 2012; Wang et al., 2005]. Applicable also for task-related functional imaging, functional ASL (fASL) is potentially a more direct marker of neuronal activity than standard BOLD functional MRI [Jin and Kim, 2008; Obata et al., 2004; Raoult et al., 2011]. Several studies have assessed the reproducibility and reliability of ASL-based quantitative results, with the aim to determine characteristic perfusion values of brain regions [Floyd et al., 2003; Lee et al., 2009; Wang et al., 2011]. At 1.5T, the random noise affects the reproducibility of measurements more than within-subject variability [Jahng et al., 2005] while, at the 3T, the SNR is significantly improved. Petersen et al. [2010] recently published a broad multicenter study on the reproducibility of quantitative ASL at 3T with 284 subjects. The mean gray matter CBF was reported to be 47.4 ± 7.5 ml/100 g/min with a within-subject standard deviation over two sessions (3- to 10-days apart) of 5.3 ml/100 g/min. The basal CBF varies substantially, not only between subjects and sessions, but also between brain regions, as does the label arrival time [Gallichan and Jezzard, 2008, 2009]. However, the normalized regional perfusion is highly reliable when measured on separate days [Pfefferbaum et al., 2010] and the relative distribution of CBF in various parts of the brain at rest is consistent and reproducible [Petersen et al., 2010; Wang et al., 2011]. Functional ASL studies have shown a high activation-related signal increase during motor and visual tasks. A signal increase of $57.3\% \pm 5.8\%$ [Raoult et al., 2011] and $39.5\% \pm 6.9\%$ [Tjandra et al., 2005] for motor tasks and $72.9\% \pm 28.8\%$ [Leontiev and Buxton, 2007] for visual tasks was reported. ASL was proven to detect signal changes during a visual-motor task with a very low task frequency [Borogovac et al., 2010]. This was demonstrated on a block-design experiment with two sessions 30 days apart. The activated region obtained using the OFF phase from the first session and the ON phase from the later session and vice-versa had size comparable to the regions detected from individual sessions [Borogovac et al., 2010]. It was also shown that normalized CBF values can be used to identify regions of the brain involved in visual tasks by comparing two groups of healthy subjects with and without visual stimulus [Aslan and Lu, 2010]. The aim of this study is to further analyze the possibility to use baseline CBF group comparison to detect motor-task activation, to compare the results with a standard fMRI block-design experiment and thus to see potential limitations of using only the ON phase. Contrary to Aslan and Lu, a larger control group is used and individual subject to group comparison is performed as would be the preferred mode to study individual subject pathologies. Such a "template approach" is commonly used in nuclear medicine to detect focal variations of a quantitative parameter obtained for one patient by comparing it to the "mean image" of several subjects [Morbelli et al., 2008]. Also, the results were compared with the results of a standard block-design fMRI experiment. Besides, means to improve the quality of detections were also investigated. Indeed, before constructing a template, the perfusion data needs to be spatially normalized. The standard spatial normalization to MNI template provides suboptimal results and we therefore tested if an alternate spatial normalization such as DARTEL [Ashburner, 2007] could improve activation detection. Yet, the spatial resolution of ASL is relatively low and most pixels contain both GM and WM tissue. Thus, given that the ASL signal mainly comes from the GM tissue, the signal intensity in ASL images depends on the volume ratio of GM and WM tissues in each pixel. The GM-to-WM perfusion ratio was reported to be on average three in adults and almost four in children [Biagi et al., 2007]. Asllani et al. [2009] measured the WM perfusion to be 3.5 times smaller than the GM perfusion in elderly subject and 3.9 times smaller in young population. Therefore, partial volume effects (PVE) can significantly affect the CBF. Partial volume correction algorithm was first introduced to ASL by Asllani et al. [2008a] and was shown to improve the detection of visual-motor task by Borogovac et al. [2010]. Four different approaches were tested and compared, using spatial normalization to MNI and DARTEL, with and without PVE correction. To illustrate its potential clinical usefulness, the method was then used to detect hypoperfusion in a single epileptic patient presenting a temporal dysplasia. To summarize, the main contributions of the paper are the following: the CBF template is constructed using DARTEL registration and PVE-correction, hyperperfused regions in motor-related tasks are detected using the template at the individual and at the group level and the results are compared with the results of a standard GLM analysis of block-design ASL experiment.

MATERIALS AND METHODS

Study Design

Thirty-seven healthy volunteers gave written informed consent to be enrolled in the study. The subjects were divided into two groups. Twenty-five subjects were included in the first group (control) (14 women and 11 men, mean age 31.6 ± 8.3 years) for the evaluation of basal perfusion. The second group (functional) consisted of 12 subjects (7 women and 5 men, mean age 28.6 ± 2.7 years) for motor activation-related perfusion evaluation. All the subjects in the second group were strongly right-handed (mean 92.5% according to the "Edinburgh Handedness Inventory" [Oldfield, 1971]).

Imaging Protocol

MR imaging was performed on a 3T MRI scanner (Magnetom Verio, Siemens, Erlangen, Germany) with a 32-channel head coil. Anatomical high resolution 3D MPRAGE T_1-weighted images were obtained for all subjects with the following parameters: field-of-view (FOV) 256 × 256 mm^2, acquisition matrix 256 × 256, 160 sagittal slabs, voxel size 1 × 1 × 1 mm^3, TR/TE/TI 1900/2.98/900 ms, flip angle 9° and acquisition time 4 min 26 s.

Rest perfusion images of control group were acquired using "quantitative imaging of perfusion with a single subtraction, with thin-slice TI1 periodic saturation" (Q2TIPS) with a "proximal inversion with a control for off-resonance effects" (PICORE) labeling technique [Luh et al., 1999; Wong et al., 1997]. The nine slices were acquired with a 7-mm slice thickness and an inter-slice gap of 0.7 mm. The slices were acquired in the AC-PC plane with the third slice passing through the AC-PC plane. The 100-mm thick PICORE labeling slab was positioned 29.5 mm below the lowest imaged slice. Sixty-one control and labeled images were acquired on each subject. A Q2TIPS saturation pulse (700 ms onset time and 800 ms duration) was used to delineate label duration and reduce the sensitivity of quantification to variations in blood arrival time in the brain [Luh et al., 1999; Wong et al., 1998]. The inversion time (TI) between the labeling pulse and the beginning of the readout was 1,700 ms for all subjects (values 1,500 and 1,800 ms that are used for similar PASL fMRI experiments [Ances et al., 2008; Perthen et al., 2008; Raoult et al., 2011; Wang et al., 2011]). A flow-sensitive bipolar crusher gradient (4 cm s^{-1}) was applied to reduce the signal from the fast-moving arterial protons [Ye et al., 1997] immediately prior to image readout. An EPI readout scheme sequence with the following parameters was used: FOV 192 × 192 mm^2, acquisition matrix 64 × 64, in-plane resolution 3 × 3 mm^2, TR/TE 3000/25 ms, and flip angle 90°. The acquisition time was 3 min 6 s.

Functional PICORE Q2TIPS ASL images were acquired, using a motor paradigm, for all subjects in the functional group. The sequence parameters were similar to the ones of the control group except for the number of slices (8) and TE (18 ms). The slices were acquired in the AC-PC plane with a 60.9 mm supratentorial coverage volume thickness. The acquisition lasted 7 min 12 s for 143 control and labeled images. The functional paradigm used a block design with seven alternating 30 s-phases (10 control and labeled images) of rest and a right-hand flexion-extension motor task of the dominant hand at approximately 1 Hz frequency. The first 3 images were used for signal stabilization and were discarded in the processing. Therefore, each rest and action phase started with a control image. It should be noted that, due to the different Z positioning of the subjects from the control and functional groups in the MR scanner, the thickness covered by both groups was around 25 mm in the Z-direction.

Template Construction

The following workflow was used for template construction from the control group images:

1. The ASL images were corrected for motion, noise and signal inhomogeneity. The ASL images were co-registered with the segmented T_1-weighted images;
2. The CBF in each voxel was quantified [Buxton et al., 1998];
3. Partial volume correction was applied [Asllani et al., 2008a];
4. The perfusion maps were spatially normalized to the MNI template or subsequently by DARTEL registration [Ashburner, 2007];
5. Intensity normalization was performed to compensate for mean inter-subject and inter-session perfusion variations;
6. The templates were constructed.

Preprocessing

All image preprocessing steps were performed using MATLAB (MathWorks, Natick, MA) and the SPM8 toolbox. First, unintentional subject movements during ASL acquisition were compensated for by motion correction of the control and labeled images using six-parameter 3D rigid registration with a sum-of-squares-difference cost function. All control and labeled images were aligned with the first control image. The T_1-weighted images were filtered using the NL-means algorithm to remove noise [Coupé et al., 2008]. The mean ASL control image was then coregistered with the T_1-weighted image of the same subject using 3D rigid-body registration with a normalized mutual-information cost function and NEWUOA optimization [Wiest-Daesslé et al., 2007]. The inhomogeneity bias in the T_1-weighted images was corrected and the images were segmented into gray matter (GM), white matter (WM) and cerebrospinal fluid (CSF) classes using the SPM8 toolbox [Ashburner and Friston, 2005]. The tissue probability template ICBM-152 [Mazziotta et al., 1995] was used as prior information for tissue classification. The GM and WM partial-volume percentages for each pixel of the low-resolution ASL images were calculated using this high-resolution segmentation projected, using the ASL/T_1-w coregistration, on the ASL image.

Perfusion Quantification

Accurate perfusion quantification relies on precise knowledge of the equilibrium magnetization of the arterial blood. However, the latter is difficult to estimate because the standard spatial resolution is too low to image an artery without any partial volume effects. In this study, the blood magnetization was estimated by dividing the first control image values M_{T0} with the blood brain partition

coefficient λ in each pixel [Cavusoglu et al., 2009]. A standard kinetic model [Buxton et al., 1998] was then used for quantification. The values of CBF in ml/100 g/min were given by:

$$\mathrm{CBF} = \lambda\ \Delta M\ \exp(\mathrm{TI}/T_{1a})/(2\alpha M_{T0}\mathrm{TI}_{\mathrm{w}}), \quad (1)$$

where λ 0.98 ml g^{-1}, α is the inversion efficiency (estimated to 1 for PASL [Wong, 2005]), ΔM is the measured mean control-label subtraction in each pixel, T_{1a} is the T_1 relaxation time of blood (T_{1a} 1,664 ms), TI_{w} is the temporal width of the bolus (TI_{w} 700 ms), and TI is the inversion time (TI 1,700 ms).

Partial Volume Correction

The signal intensity in ASL images depends on the volume ratio of GM, WM, and CSF tissues in each pixel and can be significantly affected by partial volume effects (PVE). We therefore chose to use the T_1-weighted images and their GM/WM/CSF segmentation to better delineate the boundary between GM and WM regions in the perfusion images and consequently reduce interpolation errors during spatial normalization of the images.

The ratio of GM, WM, and CSF perfusion was estimated in each pixel (see following section). The measured value of perfusion $\Delta M(r)$ in pixel r was assumed to be equal to [Asllani et al., 2008a]:

$$\Delta M(r) = P_{\mathrm{GM}}(r)\ \Delta M_{\mathrm{GM}}(r) + P_{\mathrm{WM}}(r)\ \Delta M_{\mathrm{WM}}(r) + P_{\mathrm{CSF}}(r)\ \Delta M_{\mathrm{CSF}}(r), \quad (2)$$

where P_{GM}, P_{WM}, and P_{CSF} are volume fractions of GM, WM, and CSF in each voxel; and $\Delta M_{\mathrm{GM}}(r)$, $\Delta M_{\mathrm{WM}}(r)$, and $\Delta M_{\mathrm{CSF}}(r)$ are the values of tissue-specific perfusion. The tissue perfusion $\Delta M_{\mathrm{GM}}(r)$, $\Delta M_{\mathrm{WM}}(r)$, and $\Delta M_{\mathrm{CSF}}(r)$ was assumed to be constant in a $3 \times 3 \times 1$ voxel-neighborhood in the native ASL space (voxel size $3 \times 3 \times 7$ mm^3). The perfusion values in each pixel were obtained by solving a system of nine linear equations in the least-square sense [Asllani et al., 2008a]. The separate GM/WM/CSF perfusion values ΔM_{GM}, ΔM_{WM}, and ΔM_{CSF} were then upsampled to the T_1-weighted image space and superimposed over the high-resolution GM, WM, and CSF segmentation maps [see Eq. (2)].

Spatial Normalization

The ASL images need to be spatially normalized to allow for voxel-by-voxel inter-subject comparison of perfusion values. Because the resolution of the ASL images is low, it is more accurate to align the perfusion images of different subjects via their high-resolution T_1-weighted images. Two targets were compared for normalization, a MNI305 template and a DARTEL-based template. The GM/WM segmentation of each T_1-weighted image was coregistered to the MNI305 template [Evans et al., 1993]. The DARTEL registration method was chosen for its convenient and public-available implementation [Ashburner, 2007]. The DARTEL algorithm takes all the segmented T_1-weighted images normalized to the MNI305 template and realigns them to their mean GM/WM image. The GM/WM template is iteratively recreated and all the images are realigned. The joint ASL/T_1-w and T_1-w/MNI305 template transformation was used to spatially normalize all the perfusion images. The ASL images were upsampled to the same resolution as the T_1-weighted images using trilinear interpolation.

CBF Normalization

The CBF images were also normalized in order to compensate for intersubject and intersession mean perfusion variations. For each subject in the control group, the mean perfusion was measured over all pixels with GM probability exceeding 50%. The CBF images were normalized by the subject's mean GM perfusion. For each subject in the functional group, the mean CBF value used for intensity normalization was taken from the off-phase, reflecting the mean perfusion of the subject at rest. The mean CBF of both groups was measured for a common region in the spatially normalized data where the slices were fully acquired for all subjects. The images from the on-phase were taken and used to create the activated CBF maps.

Template Construction

The templates were created by computing the mean and standard deviation over the normalized CBF maps for the control group of 25 subjects.

Four different perfusion templates were created using combinations of the previously described methods:

- Template 1—MNI: perfusion images were spatially normalized to the MNI305 template;
- Template 2—MNI+PVEc: MNI normalization and partial volume correction;
- Template 3—DARTEL: perfusion images were spatially normalized to the stereotactic space using DARTEL registration;
- Template 4—DARTEL+PVEc: DARTEL normalization and partial volume correction.

Preprocessing of Functional Group Images

Functional group image preprocessing steps were performed identically to the control group image preprocessing. An additional preprocessing step was performed on functional ASL data to minimize the BOLD effect and its influence on the size of activated areas and CBF

quantification [Lu et al., 2006]. The surround subtraction strategy was used to resample the interleaved control and labeled ASL images. Thus, control and label images corresponding to the same time point and therefore containing an identical BOLD signal were subtracted before computing the perfusion weighted images [Liu and Wong, 2005; Lu et al., 2006].

CBF Quantification Evaluation

The average gray matter CBF of each group was measured in the MNI stereotactic space over all GM pixels of the whole acquired volume. Only the off-phase was considered for the functional group to exclude the activation from the comparison. The mean perfusion over the motor areas (see section "Activation detection") on the MNI spatially normalized data was measured for the functional group. Two measurements were performed where the images from the on-phase and off-phase were considered separately in order to assess the difference in blood flow caused by the motor task.

Template Comparison

To quantitatively assess the quality of the template construction framework, we performed a leave-one-out cross-correlation by inversely transforming the template to align it with the perfusion image of each subject. For each subject of the control group, the corresponding perfusion image was excluded from the template and only the 24 remaining subjects were used. The root mean squared error (RMS) between the template and the perfusion image was calculated for each subject. Subsequently for each template, the mean RMS error over the 25 subjects was calculated. For this comparison only, the two lowest slices, presenting numerous artifacts, were excluded from the analysis for all subjects. Also, the top slice was discarded because the brain coverage after normalization was not the same for all subjects due to different brain dimensions.

Activation Detection: Template Versus GLM Comparison

First, we computed the motor task-related activated areas from the block-design functional data using the standard GLM analysis implemented in SPM after spatial smoothing with a 6-mm FWHM Gaussian filter. The statistical significance was $P < 0.05$ (family-wise error correction) and the threshold on cluster size was 250 mm^3. Detected clusters in the primary and supplementary motor areas were assumed to be the ground truth. The GLM analysis was performed on the functional group on individual subjects as well as at the group level spatially normalized either to the MNI template or using DARTEL registration.

The on-phase images of the functional group were intensity normalized to create the activated CBF images reflecting subject perfusion during motor activation. These activated CBF images were compared at the individual level to each of the four perfusion templates and the Z-score was used to identify the areas of hyperperfusion. A similar approach was used at the group level. The mean of the on-phase CBF images over all the subjects of the functional group was compared with the perfusion templates to detect the areas of hyperperfusion at the group level.

The individual and group-level activated areas detected using the standard GLM analysis (FWE $P < 0.05$) were used as a ground truth and compared with the template-detected hyperperfusion areas. The true positive ratio was computed as a percentage of the template detected area size over the ground-truth (GLM-analysis) region size. Any voxel detected as hyperperfused outside of the ground-truth region within a maximum distance of 25 mm from the border of the ground-truth region was considered as false positive. The false positive ratio was computed as the area of all false positives divided by the size of the area where the false positives were considered. The receiver operating characteristic (ROC) curve was computed showing the true positive ratios of the detection as a function of the false positive ratio from 0 to 100%. The templates were compared using the area under the curve (AUC) parameter computed from the ROC curve for each template. The mean Z score over the ground-truth region was evaluated for all four templates at the individual and at the group level.

Dysplasia Detection

A 14-year-old drug resistant epileptic female patient presenting a right temporal dysplasia, which is a recognized cause of epilepsy, was also included to assess the potential for clinical use of the presented method. The 3D MPRAGE T_1-weighted and PASL perfusion images were acquired with the same parameters as for the control group. The repetition and echo time of the PASL acquisition was TR/TE = 3,000/18 ms. For clinical screening T_2-weighted images were also acquired.

A T_1-w voxel-based morphometry (VBM) analysis was used to automatically identify abnormalities [Bannier et al., 2012; Huppertz et al., 2008; Wilke et al., 2003]. The VBM results were validated based on the T_1-weighted and T_2-weighted images by a neuroradiologist and a neurologist. The template-comparison with the four templates was used to detect hypoperfused regions with Z-score > 2.

RESULTS

CBF Quantification Evaluation

The average CBF measured for the entire GM of the spatially normalized data was 49.8 ± 12.9 ml/100 g/min for the control group and 54.1 ± 8.4 ml/100 g/min for the functional group. The difference was not significant, $P = 0.11$. In the functional group, the average CBF measured

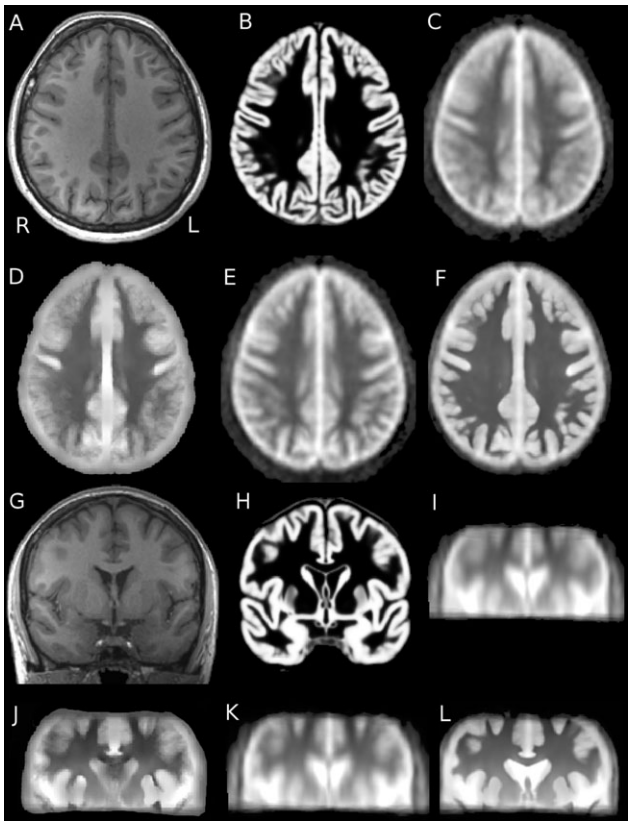

Figure 1.

Templates–axial slice. The four templates were compared with the anatomical image in axial (**A**–**F**) and coronal slices (**G**–**L**). T_1-weighted image of the first subject (A,G); mean GM segmentation of all subjects (B,H); perfusion templates MNI (C,I); MNI+PVEc (D,J); DARTEL (E,K) and DARTEL+PVEc (F,L). The GM structures were blurred in (D,E) and particularly in (C). Because of the low resolution in the axial direction, the blurring is important in coronal direction as a result of interpolation, in particular for templates MNI (C) and DARTEL (E). The partial volume correction methods reduced these artifacts as shown in (D) and especially in DARTEL+PVEc template (F). The same blurring can be observed in coronal images (I–K) and its reduction is shown in for DARTEL+PVEc (L). Note that only 9 ASL slices of thickness 7 mm were acquired. Therefore, the perfusion templates did not cover the whole brain.

on the activated primary and supplementary motor area was 53.8 ± 13.4 ml/100 g/min during the off-phase and 79.2 ± 13.6 ml/100 g/min during the on-phase. The difference was significant ($P < 0.0001$).

Template Evaluation

Mean RMS error was respectively 16.6, 16.7, 16.2, and 16.2 ml/100 g/min for templates MNI, MNI+PVEc, DARTEL, and DARTEL+PVEc. The difference between the MNI and DARTEL/DARTEL+PVEc was significant ($P < 0.05$). Figure 1 shows the comparison of the four ASL templates with a single-subject T_1-weighted image. The GM structures were blurred in particular in posterior regions and in coronal direction. Using PVE correction method, this blurring effect decreased, especially in DARTEL+PVEc template. Figure 2 shows the same aspects on subsampled templates on a single-subject CBF map.

Activation Detection: Template Versus GLM Comparison

Template activation detection enabled detection of both primary and supplementary motor areas in all subjects from the functional group. However, in two subjects the supplementary motor area was not detected using the GLM method.

The ROC curves are given in Figure 3. At maximum, the true positive ratio of the MNI template was 7.6, 4.6, and 9.6% lower than the true positive ratio of the MNI+PVEc, DARTEL, and DARTEL+PVEc template, respectively, at the individual level. At the group level, the true positive ratio of the MNI template was higher than the ratio of the MNI+PVEc in all cases and at maximum it was 9.6 and 8.1% lower than the true positive ratio of the DARTEL and DARTEL+PVEc template, respectively. The AUC was 0.81, 0.84, 0.82, and 0.84 for the MNI, MNI+PVEc, DARTEL, and DARTEL+PVEc template, respectively, at the individual level and 0.85, 0.8, 0.87, and 0.87, respectively, at the group level. The detected areas for a single subject from the functional group are shown in Figure 4. Figure 5 shows the

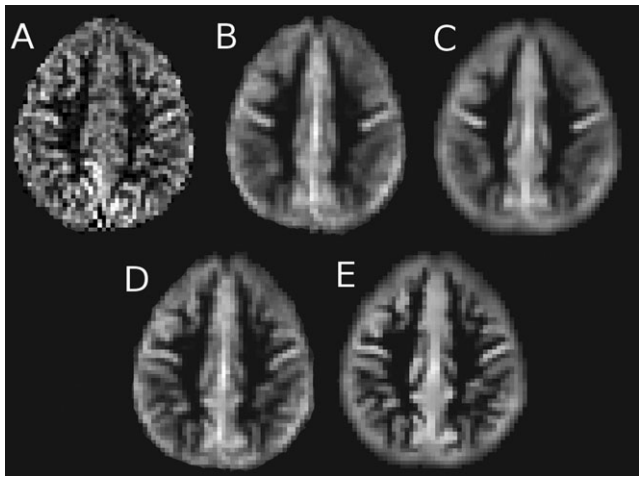

Figure 2.

Individual-subject perfusion image and reconstruction from the template. CBF map of the first subject of the control group (**A**). Templates MNI (**B**), MNI+PVEc (**C**), DARTEL (**D**), DARTEL+PVEc (**E**) were coregistered with the image (A) and subsampled to the same resolution in order to show comparison of the perfusion template and individual subject perfusion (B–E).

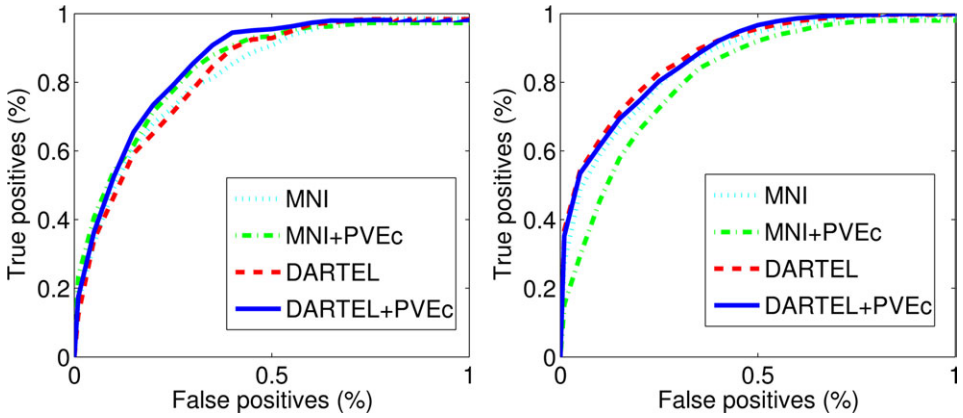

Figure 3.
Hyperperfusion detection compared with the ground truth. The true positive versus false positive ratio is shown for the four templates on individual images (left) and on group data (right). [Color figure can be viewed in the online issue, which is available at wileyonlinelibrary.com.]

group template detection overlaid over the ground-truth data obtained using the standard GLM model. The average Z score over the whole ground-truth region was 1.12, 1.15, 1.24, and 1.37 at the individual level and 1.09, 1.0, 1.42, and 1.6 at the group level for the MNI, MNI+PVEc, DARTEL, and DARTEL+PVEc template, respectively.

Dysplasia Detection

Two areas of hypoperfusion and one area of hyperperfusion were detected in the epileptic patient using the DARTEL+PVEc template, see Figure 6. The hypoperfusion in temporal gray matter (Fig. 6A) corresponded to the morphological findings. The center of gravity of this hypoperfused region was located at 1.5 mm distance from the position of the lesion detected by VBM. The hyperperfusion in thalamus (Fig. 6B) and the hypoperfusion (Fig. 6C) in the frontal gray matter are not directly related to the disease and, thus, can be regarded as false-positives in the sense of dysplasia detection. The other three templates (MNI, MNI+PVEc and DARTEL) detected with the same Z score threshold only the area of hypoperfusion in the frontal gray matter. The average Z score computed over the area of the detected temporal lesion was 1.9, 1.8, 2, and 2.5 for MNI, MNI+PVEc, DARTEL, and DARTEL+PVEc, respectively.

DISCUSSION

This study shows that an ASL template approach can detect individual and group hyperperfusions induced by motor tasks. Using DARTEL and partial volume correction in the template construction increased the accuracy of the hyperperfusion detection.

The average GM CBF of the control and functional group was 49.8 ± 12.9 and 54.1 ± 8.4 ml/100 g/min, respectively. Results for both groups are slightly higher than the mean CBF 47.4 ± 7.5 ml/100 g/min reported in the multi-center study by Petersen et al. [2010], though the difference is negligible with respect to the reported variance. Although pulsed ASL with similar labeling and bolus saturation was used in both studies, a single-TI was

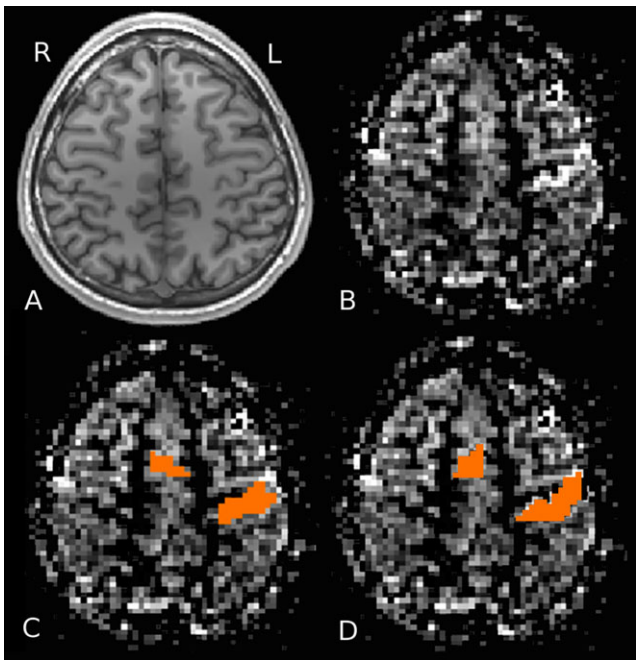

Figure 4.
Functional ASL results on an individual subject. Axial slice of a T_1-weighted image (**A**); ASL image (**B**); activated areas obtained using a standard GLM model (**C**); Hyperperfusion regions detected with the use of template DARTEL+PVEc (**D**). [Color figure can be viewed in the online issue, which is available at wileyonlinelibrary.com.]

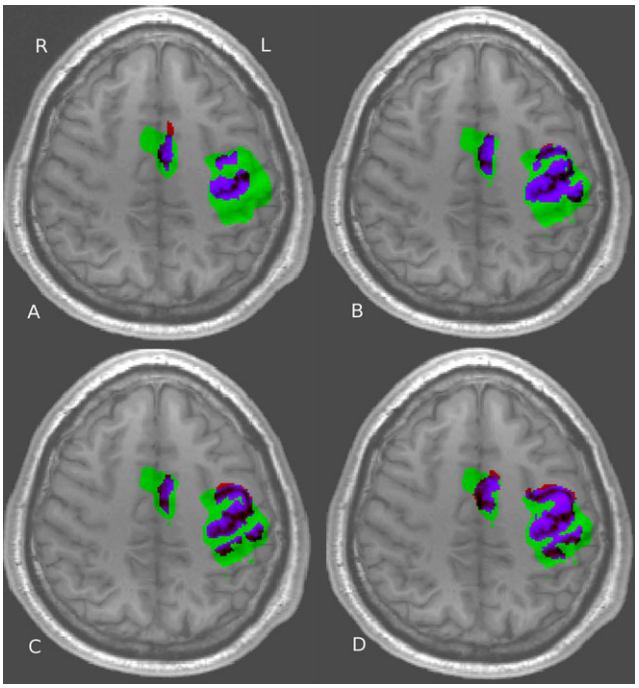

Figure 5.

Hyperperfusion detection vs. activation detection using the standard GLM model. The results are compared for the four different templates MNI (**A**), MNI+PVEc (**B**), DARTEL (**C**), and DARTEL+PVEc (**D**). The ground-truth region is in green and the activated region detected by comparison with the template is in red. Therefore, the purple region displays true positives and the red region false positives. [Color figure can be viewed in the online issue, which is available at wileyonlinelibrary.com.]

used in the present study and a multi-TI with model-free quantification was used in the multicenter study. The two types of quantification can bring different results, as for example the bolus arrival time is not estimated for the single-TI data. The model-free method was reported to give lower CBF values than a standard fit to a general kinetic model [Ho et al., 2010], which is more similar to the CBF quantification model, used in this study and can explain the difference in CBF. The difference between the individual mean values of CBF was also reported on the same study, with values varying from 39.3 to 52.7 ml/100 g/min [Petersen et al., 2010]. A significant increase in CBF was shown in the motor areas of the functional group between the off- and on-phase. This showed the modifications of local hemodynamics induced by the neuronal activity during the motor task. The detection of increased CBF induced by neuronal activity using ASL was already described by Aslan and Lu [2010]. The 47% average increase of CBF was measured in accordance with the literature findings that range from 40 to 100% [Garraux et al., 2005; Raoult et al., 2011; Wang et al., 2003] and largely depending on the selection of the region to be measured. It was slightly higher than the 35% CBF increase in motor-visual task reported by Borogovac et al. [2010].

Four templates were built and compared. Compared to MNI registration, DARTEL registration improved the perfusion contrast border between WM and GM. The reason is that DARTEL registration iteratively realigns the images of the studied group with their mean using a transformation that is less restricted than the one used in SPM to align with the MNI template. The result showed more precise alignment of the structural T_1-weighted images. It subsequently positively affected the quality of the perfusion template as can be seen from the comparison of the low-resolution perfusion images with their counterpart generated using the template. The true positive activation detection was likewise increased for both individual and group comparison. PVE correction used with DARTEL registration reduced the interpolation artifact effect by

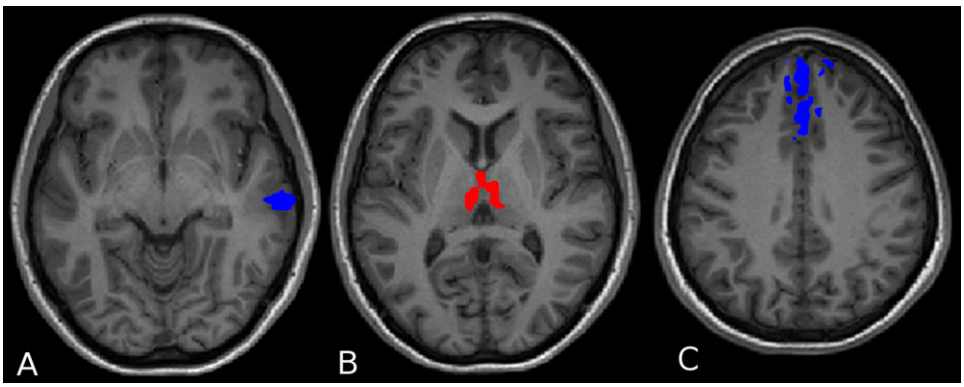

Figure 6.

Results on the epileptic patient. The hypoperfusion (**A**, **C**) and hyperperfusion (**B**) areas detected using the DARTEL+PVEc template is shown. The area in (A) is the lesion which was also detected using the VBM on the T_1-weighted images. The areas in (B) and (C) are false positive in the sense that they were not detected as the regions of dysplasia. [Color figure can be viewed in the online issue, which is available at wileyonlinelibrary.com.]

using the segmented T_1-weighted information which has significantly higher resolution than ASL images, thus allowing better localization of the perfusion sources. The outcome is mainly visible in the coronal-direction where the ASL resolution is the poorest. This should be especially useful in limiting false positive detection of hyperperfusion in white matter. The positive effect of PVE correction on true positive detection was 2.5% when using MNI normalization and 2.9% when using DARTEL normalization at the individual level. At the group level, the PVE correction for MNI normalization even decreased the true positive ratio as the MNI alignment precision is limited.

Although DARTEL+PVEc template showed increased detection and less interpolation artifacts during the spatial normalization, the PVE correction itself can smooth the CBF data by using regression on a $3 \times 3 \times 1$ neighborhood. Liang et al. [2012] has recently presented a modified least trimmed square method for partial volume correction to reduce the blurring during the regression. Also a novel method for PV ratios determination using Look-Locker sequences was proposed [Petr et al., 2013]. Both these methods can potentially further increase the detection power. The comparison of the template detection with the GLM analysis should be taken as an indicator of the possible detection power of the template and comparison to a gold standard rather than a universal proof. The reason being, that the GLM analysis itself can contain errors. The chosen threshold 0.05 FWE can create false-negatives in the GLM analysis and, thus, wrongly increase the false-positive ratio in the template detection. However, we assume that the errors in the GLM analysis are relatively small compared to the template detection and thus will not have severe effect on the relative comparison of different templates.

Following the results of Aslan and Lu [2010], the CBF of each subject was intensity normalized using the mean whole-brain perfusion prior to creating the template. The intensity normalization compensates for different mean subject perfusion levels and thus improves the quality of activation detection [Aslan and Lu, 2010]. Although the intensity-normalized data were used for inter-subject comparison, the CBF quantification step [Eq. (1)] is a necessary part of the template construction process. The reason is that the B_1-field inhomogeneity bias is partially attenuated by using a value of M_{0T} extracted from a control image with longer TR. Using raw perfusion weighted images would result in decreased quality of the results.

Both our control and activation groups were composed of young subjects. A global decrease of GM CBF of around 30% was reported in elderly population [Ances et al., 2009; Reston et al., 2007]. Brain tissue atrophy is often seen in elderly population making the GM structures thinner. This increases the negative effect of partial volume and can decrease the overall perfusion if the PVE-correction is not applied. It was shown by Asllani et al. [2009] that by using an improved processing with PVE correction, the age-related CBF difference was decreased to 15%. As no regional decrease in healthy elderly subjects was demonstrated, we think that the presented method will work similarly in elderly subjects making the added value of DARTEL+PVEc even more pronounced. However, despite the intensity normalization, use of the young subject's template to detect perfusion abnormalities needs to be evaluated.

Apart from functional MRI, the potential fields of application of the presented method are diseases presenting important regional increase/decrease of blood flow. The main constraint is the ability to obtain precise GM/WM segmentation of the whole brain and particularly of the region of interest. The method should, however, be applicable to diseases where the structure is unchanged or only affected by atrophy as for example Alzheimer and Parkinson patients, psychiatric or neuro-developmental diseases. The changes in perfusion in those patients are usually well localized and thus will not disrupt the spatial nor intensity normalization. Perfusion related changes have already been reported using ASL in Alzheimer patients [Alexopoulos et al., 2012; Asllani et al., 2008b] and Parkinson patients [Fernández-Seara et al., 2012; Melzer et al., 2011]. In these studies, no ground truth was available to validate different types of detection of perfusion changes. The approach presented here should be applicable to the same type of diseases as well. The positive effects of DARTEL and PVE correction validated with a gold-standard ground truth should further improve the precision of the stated methods. Lesion detection was demonstrated on a single epileptic patient. The DARTEL+PVEc template provided the best results, as it was the only one of the four templates that revealed the lesion at given Z-score threshold while the average Z score over the lesion was too low for the other three templates. Although two areas of hypo- and hyperperfusion were detected as well, they were distinct from the lesion and their signification remains to be investigated. In this exploratory case, we did not compare the results to other perfusion technique but only to the morphological pattern.

As the main focus was the motor cortex, a dataset with limited coverage was acquired. It should be noted that a whole-brain coverage would be essential for the aforementioned clinical applications. Acquiring ASL data with whole-brain coverage is now feasible using different acquisition techniques, in particular using 3D acquisition scheme, at different field strengths [Gai et al., 2011; Ghariq et al., 2012]. The template methodology remains the same for the whole-brain images.

In conclusion, we have shown that the individual and group motor-task related hyperperfusion can be detected by comparison with a template based on normal controls and the results are in concordance with standard block-design ASL experiments. The advantage of using DARTEL registration and PVE-correction for improving both template quality and accuracy of hyperperfusion was demonstrated.

REFERENCES

Alexopoulos P, Sorg C, Förschler A, Grimmer T, Skokou M, Wohlschläger A, Perneczky R, Zimmer C, Kurz A, Preibisch C

(2012): Perfusion abnormalities in mild cognitive impairment and mild dementia in Alzheimer's disease measured by pulsed arterial spin labeling MRI. Eur Arch Psychiatry Clin Neurosci 262:69–77.

Ances BM, Leontiev O, Perthen JE, Liang C, Lansing AE, Buxton RB (2008): Regional differences in the coupling of cerebral blood flow and oxygen metabolism changes in response to activation: Implications for BOLD-fMRI. NeuroImage 39:1510–1521.

Ances BM, Liang C, Leontiev O, Perthen J, Fleisher AS, Lansing A, Buxton RB (2009): Effects of aging on cerebral blood flow, oxygen metabolism, and blood oxygenation level dependent responses to visual stimulation. Hum Brain Mapp 30:1120–1132.

Ashburner J (2007): A fast diffeomorphic image registration Algorithm. NeuroImage 38:95–113.

Ashburner J, Friston KJ (2005): Unified segmentation. NeuroImage 26:839–851.

Aslan S, Lu H (2010): On the sensitivity of ASL MRI in detecting regional differences in cerebral blood flow. Magn Reson Imaging 28:928–935.

Asllani I, Borogovac A, Brown TR (2008a): Regression algorithm correcting for partial volume effects in arterial spin labeling MRI. Magn Reson Med 60:1362–1371.

Asllani I, Habeck C, Scarmeas N, Borogovac A, Brown TR, Stern Y (2008b): Multivariate and univariate analysis of continuous arterial spin labeling perfusion MRI in Alzheimer's disease. J Cereb Blood Flow Metab 28:725–736.

Asllani I, Habeck C, Borogovac A, Brown TR, Brickman AM, Stern Y (2009): Separating function from structure in perfusion imaging of the aging brain. Human Brain Mapp 30:2927–2935.

Bannier E, Maumet C, Pasnicu A, Ferré JC, Pasqualini E, Biraben A, Gauvrit JY, Barillot C (2012): Voxel based analysis of 3D double inversion recovery for the detection of cortical abnormalities in drug resistant epilepsy. In: Proceedings of ISMRM 2012, Melbourne, Australia. p 3244.

Biagi L, Abbruzzese A, Bianchi MC, Alsop DC, Guerra AD, Tosetti M (2007): Age dependence of cerebral perfusion assessed by magnetic resonance continuous arterial spin labeling. J Magn Reson Imaging 25:696–702.

Borogovac A, Habeck C, Small SA, Asllani I (2010): Mapping brain function using a 30-day interval between baseline and activation: A novel arterial spin labeling fMRI approach. J Cereb Blood Flow Metab 30:1721–1733.

Buxton RB, Frank LR, Wong EC, Siewert B, Warach S, Edelman RR (1998): A general kinetic model for quantitative perfusion imaging with arterial spin labeling. Magn Reson Med 40:383–396.

Cavusoglu M, Pfeuffer J, Ugurbil K, Uludag K (2009): Comparison of pulsed arterial spin labeling encoding schemes and absolute perfusion quantification. Magn Reson Med 27:1039–1045.

Chen Y, Wang DJJ, Detre JA (2011): Test-retest reliability of arterial spin labeling with common labeling strategies. J Magn Reson Imaging 33:940–949.

Coupé P, Yger P, Prima S, Hellier P, Kervrann C, Barillot C (2008): An optimized blockwise non local means denoising filter for 3D magnetic resonance images. IEEE T Med Imaging 27:425–441.

Detre JA, Leigh JS, Williams DS, Koretsky AP (1992): Perfusion imaging. Magn Reson Med 23:37–45.

Evans AC, Collins DL, Mills SR, Brown ED, Kelly RL, Peters TM (1993): 3D statistical neuroanatomical models from 305 MRI volumes. IEEE Nuclear Science Symposium and Medical Imaging Conference, pp.1813–1817.

Fernández-Seara MA, Mengual E, Vidorreta M, Aznárez-Sanado M, Loayza FR, Villagra F, Irigoyen J, Pastor MA (2012): Cortical hypoperfusion in Parkinson's disease assessed using arterial spin labeled perfusion MRI. NeuroImage 59:2743–2750.

Ferré JC, Petr J, Bannier E, Barillot C, Gauvrit JY (2012): Improving quality of arterial spin labeling MR imaging at 3 tesla with a 32-channel coil and parallel imaging. J Magn Reson Imaging 35:1233–1239.

Floyd TF, Ratcliffe SJ, Wang J, Resch B, Detre JA (2003): Precision of the CASL-perfusion MRI technique for the measurement of cerebral blood flow in whole brain and vascular territories. J Magn Reson Imaging 18:649–655.

Gai ND, Talagala SL, Butman JA (2011): Whole-brain cerebral blood flow mapping using 3D echo planar imaging and pulsed arterial tagging. J Magn Reson Imaging 33:287–295.

Gallichan D, Jezzard P (2008): Modeling the effects of dispersion and pulsatility of blood flow in pulsed arterial spin labeling. Magn Reson Med 60:53–60.

Gallichan D, Jezzard P (2009): Variation in the shape of pulsed arterial spin labeling kinetic curves across the healthy human brain and its implications for CBF quantification. Magn Reson Med 61:686–695.

Garraux G, Hallett M, Talagala SL (2005): CASL fMRI of subcortico-cortical perfusion changes during memory-guided finger sequences. NeuroImage 25:122–132.

Ghariq E, Teeuwisse WM, Webb AG, van Osch MJP (2012): Feasibility of pseudocontinuous arterial spin labeling at 7 T with whole-brain coverage. Magma 25:83–93.

Ho YCL, Petersen ET, Golay X (2010): Measuring arterial and tissue responses to functional challenges using arterial spin labeling. NeuroImage 49:478–487.

Huppertz HJ, Wellmer J, Staack AM, Altenmüller DM, Urbach H, Kröll J (2008): Voxel-based 3D MRI analysis helps to detect subtle forms of subcortical band heterotopia. Epilepsia 49:772–785.

Jahng GH, Song E, Zhu XP, Matson GB, Weiner MV, Schuff N (2005): Human brain: Reliability and reproducibility of pulsed arterial spin-labeling perfusion MR imaging. Radiology 234:909–916.

Jin T, Kim SG (2008): Cortical layer-dependent dynamic blood oxygenation, cerebral blood flow and cerebral blood volume responses during visual stimulation. NeuroImage 43:1–9.

Lee C, Lopez OL, Becker JT, Raji C, Dai W, Kuller LH, Gach HM (2009): Imaging cerebral blood flow in the cognitively normal aging brain with arterial spin labeling: Implications for imaging of neurodegenerative disease. J Neuroimaging 19:344–352.

Leontiev O, Buxton RB (2007): Reproducibility of BOLD, perfusion, and CMRO2 measurements with calibrated-BOLD fMRI. NeuroImage 35:175–184.

Liang X, Connelly A, Calamante F (2012): Improved partial volume correction for single inversion time arterial spin labeling data. Magn Reson Med C:1–7.

Liu TT, Wong EC (2005): A signal processing model for arterial spin labeling functional MRI. NeuroImage 24:207–215.

Lu H, Donahue MJ, van Zijl PCM (2006): Detrimental effects of BOLD signal in arterial spin labeling fMRI at high field strength. Magn Reson Med 56:546–552.

Luh WM, Wong EC, Bandettini PA, Hyde JS (1999): QUIPSS II with thin-slice TI1 periodic saturation: A method for improving accuracy of quantitative perfusion imaging using pulsed arterial spin labeling. Magn Reson Med 41:1246–1254.

Mazerolle EL, Beyea SD, Gawryluk JR, Brewer KD, Bowen CV, D'Arcy RC (2010): Confirming white matter fMRI activation in the corpus callosum: Co-localization with DTI tractography. NeuroImage 50:616–621.

Mazziotta JC, Toga AW, Evans A, Fox P, Lancaster J (1995): A probabilistic atlas of the human brain: Theory and rationale for its development. NeuroImage 2:89–101.

Melzer TR, Watts R, MacAskill MR, Pearson JF, Rüeger S, Pitcher TL, Livingston L, Graham C, Keenan R, Shankaranarayanan A, Alsop DC, Dalrymple-Alford JC, Anderson TJ (2011): Arterial spin labeling reveals an abnormal cerebral perfusion pattern in Parkinson's disease. Brain 134:845–855.

Morbelli S, Rodriguez G, Mignone A, Altrinetti V, Brugnolo A, Piccardo A, Pupi A, Koulibaly PM, Nobili F (2008): The need of appropriate brain SPECT templates for SPM comparisons. Q J Nucl Med Mol Imaging 52:89–98.

Obata T, Liu TT, Miller KL, Luh WM, Wong EC, Frank LR, Buxton RB (2004): Discrepancies between BOLD and flow dynamics in primary and supplementary motor areas: Application of the balloon model to the interpretation of BOLD transients. NeuroImage 21:144–153.

Oldfield RC (1971): The assessment and analysis of handedness: The Edinburgh inventory. Neuropsychologia 9:97–113.

Parkes LM, Detre JA (2004): ASL: Blood Perfusion Measurements Using Arterial Spin Labelling, In: Quantitative MRI of the Brain: Measuring Changes Caused by Disease (ed P. Tofts), John Wiley & Sons, Ltd, Chichester, UK. DOI: 10.1002/0470869526.ch13.

Perthen JE, Bydder M, Restom K, Liu TT (2008): SNR and functional sensitivity of BOLD and perfusion-based fMRI using arterial spin labeling with spiral SENSE at 3 T. Magn Reson Imaging 26:513–522.

Petersen ET, Mouridsen K, Golay X (2010): The QUASAR reproducibility study, part II: Results from a multi-center arterial spin labeling test-retest study. NeuroImage 49:104–113.

Petr J, Schramm G, Hofheinz F, Langner J, van den Hoff J (2013): Partial Volume Correction in Arterial Spin Labeling Using a Look-Locker Sequence. Magn Reson Med (in press). DOI: 10.1002/mrm.24601.

Pfefferbaum A, Chanraud S, Pitel AL, Shankaranarayanan A, Alsop DC, Rohlfing T, Sullivan EV (2010): Volumetric cerebral perfusion imaging in healthy adults: Regional distribution, laterality, and repeatability of pulsed continuous arterial spin labeling (PCASL). Psychiatry Res-Neuroim 182:266–273.

Raoult H, Petr J, Bannier E, Stamm A, Gauvrit JY, Barillot C, Ferré JC (2011): Arterial spin labeling for motor activation mapping at 3T with a 32-channel coil: Reproducibility and spatial accuracy in comparison with BOLD fMRI. NeuroImage 58:157–167.

Restom K, Bangen KJ, Bondi MW, Perthen JE, Liu TT (2007): Cerebral blood flow and BOLD responses to a memory encoding task: A comparison between healthy young and elderly adults. NeuroImage 37:430–439.

Tjandra T, Brooks JC, Figueiredo P, Wise R, Matthews PM, Tracey I (2005): Quantitative assessment of the reproducibility of functional activation measured with BOLD and MR perfusion imaging: Implications for clinical trial design. NeuroImage 27:393–401.

Wang J, Aguirre GK, Kimberg DY, Roc AC, Li L, Detre JA (2003): Arterial spin labeling perfusion fMRI with very low task frequency. Magn Reson Med 49:796–802.

Wang Z, Wang J, Connick TJ, Wetmore GS, Detre JA (2005): Continuous ASL (CASL) perfusion MRI with an array coil and parallel imaging at 3T. Magn Reson Med 54:732–737.

Wang Y, Saykin AJ, Pfeuffer J, Lin C, Mosier KM, Shen L, Kim S, Hutchins GD (2011): Regional reproducibility of pulsed arterial spin labeling perfusion imaging at 3T. NeuroImage 54:1188–1195.

Wiest-Daesslé N, Yger P, Prima S, Barillot C (2007): Evaluation of a new optimization algorithm for rigid registration of MRI data.In SPIE Medical Imaging 2007: Image Processing, San Diego, USA.

Wilke M, Kassubek J, Ziyeh S, Schulze-Bonhage A, Huppertz HJ (2003): Automated detection of gray matter malformations using optimized voxel-based morphometry: A systematic approach. Neuroimage 20:330–343.

Wong EC (2005): Quantifying CBF with pulsed ASL: Technical and pulse sequence factors. J Magn Reson Imaging 22:727–731.

Wong EC, Buxton RB, Frank LR (1998): Quantitative imaging of perfusion using a single subtraction (QUIPSS and QUIPSS II). Magn Reson Med 39:702–708.

Ye FQ, Mattay VS, Jezzard P, Frank JA, Weinberger DR, McLaughlin AC (1997): Correction for vascular artifacts in cerebral blood flow values measured by using arterial spin tagging techniques. Magn Reson Med 37:226–235.

Yousry TA, Schmid UD, Alkadhi H, Schmidt D, Peraud A, Buettner A, Winkler P (1997): Localization of the motor hand area to a knob on the precentral gyrus. A new landmark. Brain 120:141–157.